Environmental and Experimental Botany 200 (2022) 104906

Contents lists available at ScienceDirect

Environmental and Experimental Botany

journal homepage: www.elsevier.com/locate/envexpbot

Root cell wall remodeling mediates copper oxide nanoparticles phytotoxicity on lettuce (*Lactuca sativa* L.)

Xinyu Guo [a], Jipeng Luo [a], Ran Zhang [c], Hairong Gao [c], Liangcai Peng [c], Yongchao Liang [a], Tingqiang Li [a,b,*]

[a] Ministry of Education Key Laboratory of Environmental Remediation and Ecological Health, College of Environmental and Resource Sciences, Zhejiang University, Hangzhou 310058, China
[b] Zhejiang Provincial Key Laboratory of Agricultural Resources and Environment, Hangzhou 310058, China
[c] Biomass and Bioenergy Research Centre, Huazhong Agricultural University, Wuhan 430070, China

ARTICLE INFO

Keywords:
Root growth
Copper oxide nanoparticles
Pectin
Cell wall thickness
Xyloglucan endotransglycosy/hydrolase

ABSTRACT

Root cell wall (RCW) remodeling induced by copper oxide nanoparticles (CuO NPs) and its consequences for root growth of lettuce (*Lactuca sativa* L.) were investigated in this study. The results showed that a low concentration of CuO NPs (5 mg L^{-1}) stimulated reactive oxygen species (ROS) signaling, led to the degradation of pectin by H_2O_2, and promoted root elongation by 22.1% by triggering RCW loosening. However, under treatment with a high concentration of CuO NPs (450 mg L^{-1}), the unordered distribution of pectin homogalacturonan enhanced cell wall adhesion. Also, the increased xyloglucan and the decreased xyloglucan endotransglycosylase/hydrolase (XTH) activities caused cell wall stiffening, making it difficult for lettuce roots to extend. Meanwhile, the contents of hemicellulose and low-methylated pectin were increased remarkably due to the downregulation of the encoding genes *XTH15*, *XTH17*, *XTH31* and the upregulation of *PME3*, which provided abundant binding sites of RCW with CuO NPs. In addition, the accelerated development of the apoplastic barrier and root lignification blocked the absorption of CuO NPs, and the endodermal cell walls were doubled in thickness, greatly enhancing their retention capacity to CuO NPs. Taken together, the above findings suggest that CuO NPs have concentration-dependent effects on lettuce roots, which are associated with plant tolerance and mediated by RCW remodeling.

1. Introduction

Copper oxide nanoparticles (CuO NPs) with the dual properties of metal and nanoparticles are widely used in catalysts, sensors and antimicrobial formulations (Gomez et al., 2021). CuO NPs can enter the soil-plant system through polluted sediments, groundwater circulation and atmospheric deposition, making plants the potential carriers for the migration, transformation and bioaccumulation of nanoparticles (Peng et al., 2015; Xiong et al., 2017). In recent decades, several reports have focused on the morphological changes and toxic impacts of CuO NPs, as well as its absorption, translocation and distribution in plants (Dimkpa et al., 2013; Deng et al., 2020). However, few have explored the anatomical structural changes of plant roots, as well as their cellular responses to CuO NPs.

Numerous studies have confirmed that root growth is inhibited under abiotic stress (Kazan, 2013; Kopittke and Wang, 2017). Interestingly, different types and concentrations of metallic nanoparticles (MNPs) may cause various effects on root growth (Verma et al., 2018; Wang et al., 2020). It was found that a high concentration of CuO NPs (greater than 100 mg mL^{-1}) induced oxidative stress in wheat (*Triticum aestivum*), rice (*Oryza sativa* L.) and Cu hyperaccumulator *Elsholtzia splendens*, which in turn inhibited root growth and biomass (Adams et al., 2017; Shi et al., 2014). In contrast, several reports have shown that low concentrations of MNP (below 10 mg mL^{-1}) have a positive effect on root growth, as observed in TiO_2 NPs and Au NPs in *Arabidopsis thaliana* (Lenaghan et al., 2013; Jain et al., 2014), as well as ZnO NPs to *Cucumis sativus* seedlings (Moghaddasi et al., 2017). Therefore, were these MNP-induced changes related to root cell wall (RCW) remodeling? Because it is well known that RCW loosening is essential for root growth, especially elongation (Van Sandt et al., 2007). In general, most cell wall polysaccharides are subjected to some degree of hydrolyzation, resulting in structural loosening and reduced

* Correspondence to: College of Environmental and Resource Sciences, Zhejiang University, Hangzhou 310058, China.
E-mail address: litq@zju.edu.cn (T. Li).

https://doi.org/10.1016/j.envexpbot.2022.104906
Received 30 January 2022; Received in revised form 5 May 2022; Accepted 8 May 2022
Available online 13 May 2022

intercellular adhesion between cell walls (Kim et al., 2014). Furthermore, cell wall loosening and stiffening usually require the participation of a variety of enzymes including xyloglucan endotransglycosylase/hydrolase (XTH), which catalyze the assembly and hydrolysis of xyloglucan via the regulation of *XTH* encoding genes, thus promoting the extension of roots (Zhu et al., 2012). Nevertheless, compared with the extensive research on heavy metals (HMs) on root growth, little is known about whether the effects of MNPs on root elongation are related to RCW remodeling, needless to exploring the underlying mechanism.

RCW not only plays an important role in regulating root development, but also acts as an effective barrier for plants to cope with MNPs (Wu et al., 2020; Molnár et al., 2020). Recent studies have shown that the CuO NPs absorbed by roots are mainly localized in the cell wall and intercellular spaces (Yuan et al., 2016; Deng et al., 2020). However, whether NPs can penetrate the RCW of plants and bind to active cell wall polysaccharides is still controversial, and may depend on the size and stability of nanoparticles (Verma et al., 2018). For instance, some studies suggested that TiO_2 (smaller than 5 nm) and CuO NPs (smaller than 20 nm) caused mechanical damage to the cell wall and passed through this blocker (Kurepa et al., 2010; Wang et al., 2012). Another puzzle at present is what are the specific responses of RCW to NPs? Generally, plants can protect their cells against abiotic stress by remodeling the composition and structure of the cell wall, e.g., forming an effective layer with stronger binding ability (polysaccharide fixing and cell wall thickening, Krzesłowska et al., 2016; Guo et al., 2021) or preventing apolastic transportation (Barberon et al., 2016) and enhanced root lignification (Nair and Chung, 2015; Kováč et al., 2018). Unfortunately, when faced with different concentrations of CuO NPs, the molecular mechanisms of RCW remodeling are poorly understood, especially the changes in cell wall polysaccharides that are involved in binding metal ions and determining the growth of plants.

Leafy vegetables are a nutritious and essential food for the human diet (Liu et al., 2018), whereas the widely used CuO NPs affect the growth of plants, accumulate in edible shoots, and consequently threaten the safety of agricultural products (Verma et al., 2018; Gomez et al., 2021). Therefore, it is necessary to understand the response and underlying mechanism of vegetable crops to CuO NPs. Using lettuce (*Lactuca sativa* L.) as research objects, this study aims to (1) investigate the effect of different concentrations of CuO NPs on root development; (2) identify the variation of RCW composition and structure upon CuO NPs exposure; and (3) reveal the predominant mechanism of RCW remodeling in response to CuO NPs.

2. Materials and methods

2.1. Preparation and characterization of CuO NPs

The particle size and morphology of CuO NPs (Sigma-Aldrich, USA) were characterized via transmission electron microscope (TEM, Hitachi, Ibaraki, Japan). The Zeta potential of different concentrations of CuO NPs in (Hoagland) nutrient solution (pH 5.85) was determined using a Zetasizer-Nano ZS instrument (Malvern Nano-ZS90, England) after a 30 min sonication and a 1 h post-sonication waiting time. The TEM analysis of CuO NPs in suspension indicated that nanoparticles were spherical, and the average particle size is about 35.6 ± 3.1 nm ($n = 50$; Fig. S1). The hydrodynamic diameter and zeta potential of CuO NPs in the nutrient solution were 515 ± 52 nm and 20.5 ± 3.3 mV, respectively (Table S3). With the concentration increased, the absolute value of zeta potential enhanced gradually, the hydraulic diameter of dispersed particles decreased and the system became more stable. The other physicochemical properties are presented in Fig. S1 and Table S3.

Different concentrations of CuO NPs (5, 50, 150, 450 mg L^{-1}) and 450 mg L^{-1} CuO bulk particles (CuO BPs) nutrient solutions were placed in the dark. The suspensions were collected at 1, 8, 24, 48, 72, 120 h by a centrifuge (at 6000 g for 30 min), the dissolved Cu concentration of CuO NPs was then determined by inductively coupled plasma-mass spectrophotometer (ICP-MS, Agilent 7500a, USA) after being filtered through 0.22 μM filter membrane according to previous protocols (Peng et al., 2015).

2.2. Plant cultivation and experiment design

Lettuce seeds were surface sterilized (2% H_2O_2 solution for 10 min) and soaked in deionized water for 2 h. Finally, seeds were sowed in clean and moist quartz sand, covered with a layer of fine sand and placed in the plant incubator. The incubator was set to 14/10 h day/night alternate cycle, the relative humidity and the temperature were controlled as 70% and 24 °C respectively. After germination, healthy and uniform plants were transferred to 1/4 Hoagland nutrient solution (Table S1) for one week. After per-culturing, plants were transferred into full-strength Hoagland nutrient solution supplied with 0 (CK) or different concentrations of CuO NPs (5, 50, 150, 450 mg L^{-1}) for 7 d, and there was no application to leaves. The root length was measured by a ruler at 9:00 AM every day. At the end of the treatment, 4 plants were randomly chosen, and separated into roots and shoots. Then roots were carefully washed with 20 mM ethylenediamine tetra-acetic acid disodium salt solution and deionized water to remove the CuO NPs that absorbed on the roots surface (Kopittke et al., 2009). The dry weight of roots and shoots were determined after drying in an oven at 85 °C for 72 h.

2.3. SEM-EDS observation

The distribution of CuO NPs in lettuce roots was observed via the scanning electron microscope (SEM, FEI QUANTA FEG 650), and surface element analysis was conducted at the same locations by using energy dispersive X-ray spectroscopy (EDS, EDAX Inc. Genesis XM). Fresh roots (approximately 0.2–0.8 mm from root tip) were cut into 10–15 μm sections by using a freezing microtome (SLEE MTC, Germany). Gold-palladium was used to wrap the dehydrated cross sections by Hitachi Model E-1010 ion sputter for 5 min and images were observed in Hitachi Model TEM-1000 SEM and INCA100EDS (Oxford shujire, UK).

2.4. Cell wall assay

2.4.1. Cell wall extraction, fractionation and measurement

At the end of the treatment, the RCW of lettuce was extracted and fractionated into pectin, hemicellulose 1, hemicellulose 2, cellulose and lignin (Yang et al., 2011; Guo et al., 2022). Subsequently, different RCW fractions were prepared and digested in HNO_3-H_2O_2 (5:1, v/v) for 8–10 h. ICP-MS (Agilent 7500a, USA) was applied for Cu assay.

The uronic acid contents in pectin were measured spectrophotometrically at a wave length of 520 nm according to Blumenkrantz and Asboe-Hansen (1973). The total sugars contents of hemicellulose 1, hemicellulose 2 and cellulose were calculated by phenol sulfuric acid method (Dubois et al., 1956). Lignin content of roots was calculated according to the method we used before (Guo et al., 2021) and expressed as a percentage of cell wall residue (CWR) dry weight (Van et al., 2013).

2.4.2. Monosaccharide determination by gas chromatography-mass spectrometer (GC-MS)

RCW polysaccharides fractions were dialyzed for 48 h (replace the distilled water every 2 h) after the neutralization (pH=7) with acetic acid. Then the monosaccharide composition of pectin, hemicellulose 1 and 2 were determined with GC-MS (including acid hydrolysis and derivatization). Chemical reagents, monosaccharide standards used in this experiment as well as GC-MS analytical conditions were previously described by Guo et al. (2020). GC-MS-QP 2010 Plus was used for data analysis.

2.4.3. Immunofluorescence localization of pectin and hemicellulose

Fresh roots of different segments were cut into thin slices of 10 μm by a freezing microtome (SLEE MTC, Germany), then incubated with 0.2%

bovine serum albumin (BSA) solution for 1 h under darkness. Then samples were incubated with polysaccharide monoclonal antibody (LM19 bind to pectic homogalacturonan, JIM5 bind to unesterified homogalacturonan, JIM7 bind to highly methylesterified homogalacturonan, and CRCCM99 bind to xyloglucan, all monoclonal antibodies were diluted with 0.2% BSA blocking solution) for about 2 h (more information refer to Table. S4). The preparations were washed with PBS for three times, subsequently, labeled with secondary fluorescent antibody in the dark for 2 h (Alexa Fluor 488 anti-Rat Ig G (H+L), Invitrogen, A11006 combined with JIM series; Alexa Fluor 488 anti-mouse Ig G (H+L), Invitrogen, A11001 combined with CCRC series). These two kinds of secondary antibodies were combined with fluorescein isothiocyanate (FITC) and diluted 200 times with PBS. Finally, these glass slide samples were washed with PBS buffer for three times and captured under a confocal fluorescence microscope (Nikon eclipse 80i, Japan).

All processes were observed by microscopy with the same exposure parameter and samples without incubated with primary antibodies were used as control.

2.4.4. Dye of cellulose and lignin

Cross-sections of fresh roots (20–30 μm, approximately 0.5–0.8 mm from root tips) were counterstained with Calcofluor white (Sigma, cellulose visualization) and phloroglucinol/HCl (v/v=1:1) solution (lignin visualization) separately. Images were obtained by fluorescence microscope under bright field (for lignin) and fluorescence field (excitation wavelength is 330–385 nm, for cellulose).

2.4.5. TEM observation and immunolabelling of cell wall polysaccharide

Immuno-gold colloid techniques based on antigen-antibody specific binding can be used to observe cell wall polysaccharides in situ (Krzesłowska et al., 2016). Herein immunolabelling procedure was carried out according to Guo et al. (2021). Ultra-thin root sections (80 nm) were incubated in blocking buffer (EMS, Hatfield, PA) for 30 min at 37 °C, and then were move into the primary antibody (LM19 bind to pectic homogalacturonan) at 1:100 for 3 h at 30 °C. Subsequently, they were washed three times in deionized water for 5 min at each step, and labeled with secondary antibody (anti-rat IgG-gold, 10 nm particles) at 1:20 for 2 h at 37 °C, continue washing again in deionized water. Finally, 2% uranyl acetate and 2% lead citrate were applied for grids with different labelling treatments for 15 min. Spectra were obtained under Hitachi Model H-7650 TEM (Hitachi, Ibaraki, Japan), with each treatment had 4 repetitions. Thickness of RCW and the density of gold labeling in regions of TEM images were calculated by the ImageJ software.

2.5. Fluorescence localization of Cu on the cross sections of root

Roots treated with 5 and 450 mg L^{-1} CuO NPs treatment for 7 d were cut into cross-sections (20–30 μm) using a freezing microtome (MTC; SLEE medical GmbH, Mainz, Germany), then stained with a selectively fluorescein-based colorimetric probe for detecting Cu^{2+} (soluble in DMF: CH_3CN, v/v=1:1, Helison Biotechnology Co., Ltd., Xiamen, China) in the dark for 10 min, and washed three times with PBS buffer for 5 min (Zhang et al., 2014). Confocal fluorescence microscope (Nikon eclipse 80i, Japan) was used to investigate the spatial distribution of Cu, samples unstained with Cu^{2+} probe were used as control.

2.6. Biochemical analysis

2.6.1. Detection of ROS, H_2O_2 and $O_2^{\bullet-}$

The H_2O_2 contents of root samples were calculated by detecting titanium-peroxide complex formation according to Sun et al. (2014). The $O_2^{\bullet-}$ contents were measured as described by Liu et al. (2007) as following: 0.5 g roots were initially ground and extracted in 2 mL of 65 mM phosphate buffer (pH 7.8). The homogenate was centrifuged at 5000 g for 10 min, and the supernatant was mixed with 0.9 mL phosphate buffer (pH 7.8) and 0.1 mL of 10 mM hydroxylamine hydrochloride, and incubated at 25 °C for 20 min. Then, 1 mL anhydrous p-aminobenzene sulfonic acid and 1 mL 1-naphthylamine were added to the mixture. The absorbance was calculated at 540 nm after adding 3 mL n-butyl alcohol. Meanwhile, total reactive oxygen species (ROS) and $O_2^{\bullet-}$ accumulation in root tips were observed via using the fluorescent probe 2′,7′-dichlorofluorescin diacetate (DCFH-DA, Beyotime, Jiangsu, China) and dihydroethidium (DHE, Sigma-Aldrich) as described by Jones et al. (2006) and Sun et al. (2014). Root tips of untreated (CK) and treated plants were cut off and incubated respectively with 200 μL DCFH-DA (10 μM) and DHE (10 μM) for 20 min in dark, then washed three times with PBS buffer for 5 min. Images of staining roots were obtained by a confocal fluorescence microscope (Nikon eclipse 80i, Japan).

2.6.2. Determination of auxin content

Take fresh root samples of lettuce with different treatments, wash and grind them into powder with a grinder. Then, weigh 50 mg samples and add 10 μL internal standard mixture with a concentration of 100 ng mL^{-1}. Add 1 mL of methanol/water/formic acid (15:4:1, v/v/v) extractant and mixed well. After vertexing for 10 min, samples were centrifuged at 12,000 r min^{-1} for 5 min under 4 °C, and supernatants were taken into a new centrifuge tube for concentration. Then use 100 μL 80% methanol solution for re-dissolving, all samples were filtered over 0.22 μM water filtration membrane, placed in the injection bottle for Ultra Performance Liquid Chromatography-Tandem Mass Spectrometry (LC-MS/MS, QTRAP 6500 +, SCIEX, USA) analysis.

2.6.3. Enzymatic antioxidants

The PME activity was determined as described by Li et al. (2015) with minor modifications. After treatment, the cell wall of lettuce root was extracted and dried (refer to *2.4.1*), then a 20 mg RCW sample was mixed with 500 μL 1 M L^{-1} sodium chloride solution (pH=6.0), and the supernatant was obtained by centrifugation after ice-bathing (1 h). Mixed 50 μL supernatant with alcohol oxidase (10 μL, diluted 100 times with PBS buffer, pH 7.5) and 0.64 mg mL^{-1} pectin (100 μL, Sigma, the degree of methyl esterification is 90%), incubated at 30 °C for 10 min, then add 200 μL 5 mg mL^{-1} purpald solution (soluble in 0.5 M NaOH), shaked and incubated in 30 °C for 30 min, finally add 550 μL deionized water and measured at 550 nm spectrophotometrically.

Superoxide dismutase (SOD), peroxidase (POD), catalase (CAT) and ascorbate peroxidase (APX) activity kits were from Nanjing Jiancheng Bioengineering Institute. The double antibody sandwich method by ELISA Kit (Jiang Lai Biotechnology Co., Ltd. Shanghai, China) was used to determine the activities of xyloglucan endohydrolase (XEH) and xyloglucan endotransglycosylase (XET) according to our previous studies (Guo et al., 2020). About 0.1 g fresh roots were cut off and frozen by liquid nitrogen immediately to be pulverized, then added 0.9 mL PBS (pH=7.4). The sample was centrifuged and the supernatant was used to assay enzyme activity by following steps in accordance with manufacturer's instructions.

2.7. PI dye

Propidium iodide (PI, Sigma-Aldrich) is used as an apoplastic tracer according to Naseer et al. (2012). Based on the quantification protocol of Alassimone et al. (2010), the penetration of PI into stele was used to observe the function of apoplastic barriers in roots. Root tips were cut into 20 μm cross-sections using a freezing microtome (SLEE MTC, Germany), then stained with 10 μg mL^{-1} PI solution for 5 min in the darkness, then the root tips were rinsed in deionized water for 2 min. The PI staining was observed with a confocal laser scanning microscope (FV3000, Olympus; Japan). The excitation and emission wavelengths were 559 nm and 570–670 nm, respectively. Moreover, the number of dead cells of root cap and the length of elongation zone cells was calculated by ImageJ software.

2.8. Real-time quantitative PCR analysis

Total RNA of plants roots was extracted with a Column Plant RNAout (OMEGA, Beijing, China), then the isolated RNA was reversed into cDNA and amplified into DNA by ordinary polymerase chain reaction (PCR) procedure. Relative gene expression levels were determined by SYBR Green qPCR Master Mix (Takara Bio Inc., Shiga, Japan) and performed using Applied Biosystems 7900HT Fast Real-Time PCR System (Applied Biosystems, USA). The relative gene expressions were calculated via $2^{-\Delta\Delta}$CT methods (Pfaffl, 2001) and *LsACTIN* was used as an internal control. The primers sequences for the target gene (*GAUT1, PME3, PME17, XTH15, XTH17, XTH31*) are listed in Supplementary Table 3.

2.9. Statistical analysis

All data were analyzed by using SPSS (version 20.0, SPSS Inc., Chicago, IL, USA). Duncan' s multiple range test was applied to compare differences between treatments at $P < 0.05$. Graphical works were generated via ImageJ, OMNIC and OriginPro 8.0 software.

3. Results

3.1. Root growth

Through dynamic monitoring of lettuce root growth, we found that a low concentration of CuO NPs significantly promoted root elongation by 22.1% at the end of 7-D-treatment (Fig. 1A, B, $P < 0.05$). With the increase of CuO NPs concentrations, roots growth was gradually negatively affected and their length were completely inhibited upon 450 mg L^{-1} CuO NPs exposure, an about 70% of decrease on biomass were observed as well (Fig. S4). Under 450 mg L^{-1} CuO NPs treatment, the root was seriously deformed and the root surface was oxidized and browned, dead cells appeared in the root tip, the length of elongation zone cell was significantly shortened by 28% compared with CK, also a

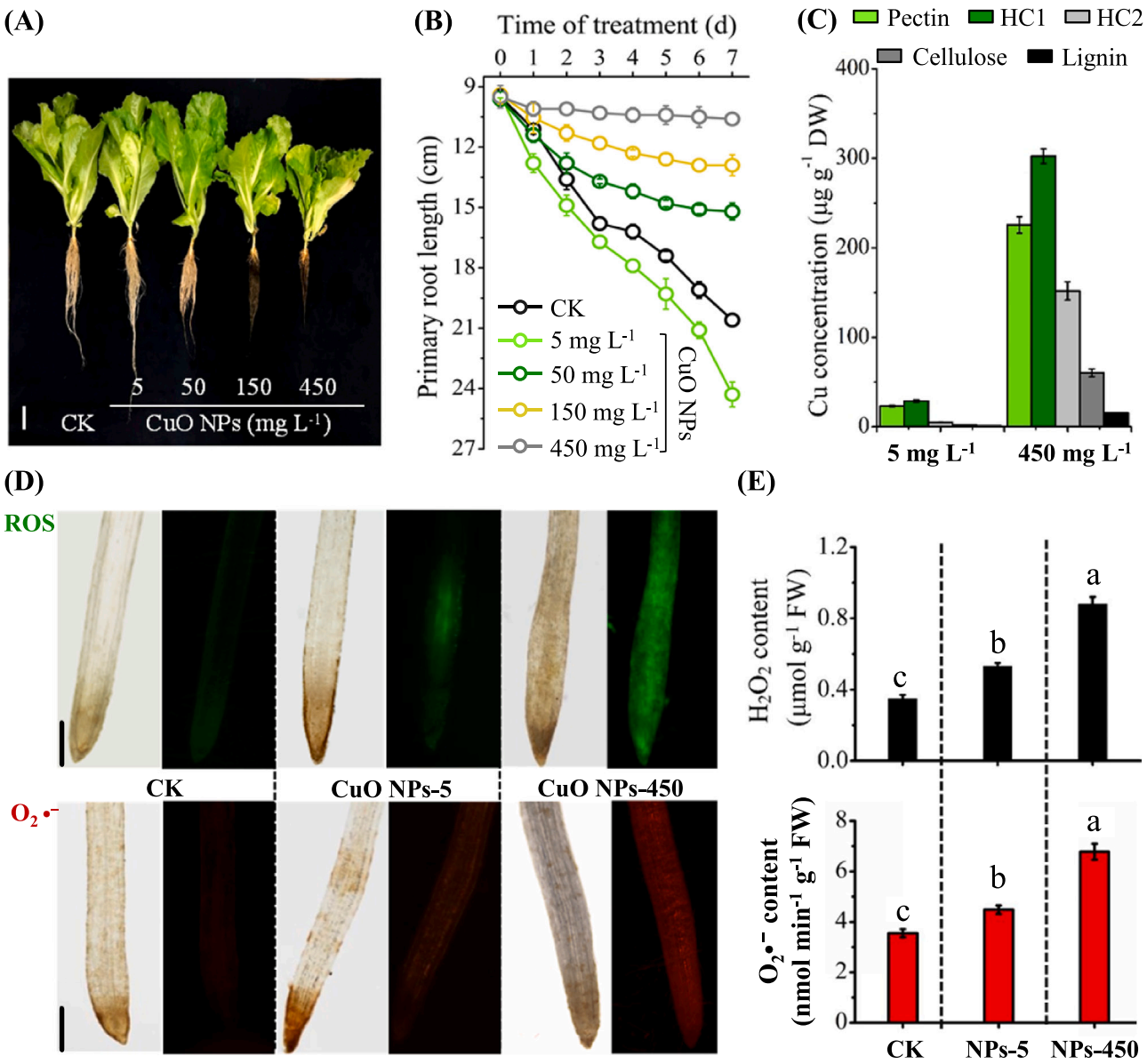

Fig. 1. Effects of different levels of CuO NPs on lettuce roots: (A) The photographs of plants. Scale bars: 5 cm. (B) Primary root length of plants during 7-day-supply with different concentrations of CuO NPs (C) Cu concentration in pectin, hemicellulose 1 and 2 as well as cellulose and lignin of RCW. Meanwhile, plants were treated with different levels of CuO NPs for 7 d, then root tips were collected and used for detecting ROS and superoxide ($O_2^{\bullet-}$) accumulation (D), meanwhile, H_2O_2 and $O_2^{\bullet-}$ contents were determined by using spectrphotometry (E). Values represents means ± SD ($n = 4$) and different letters indicate significant differences ($P < 0.05$) among the treatments. The scale bar represents 0.5 cm. FW: fresh weight.

large number of cells above the root tip were incomplete and fell off (Fig. 3B).

3.2. ROS and antioxidant system

Under 450 mg L^{-1} CuO NPs treatment, the concentrations of H_2O_2 and $O_2^{\bullet-}$ increased by 151.4% and 76.1% than control, respectively (Fig. 1D, E, Table S5), which may degrade the polysaccharide distribution profiles of intercellular space and affect RCW loosening as well as the root elongation. On the other hand, compared with CK, enzyme activities of SOD, POD, CAT and APX which could protect against ROS were increased by 216.5%, 52.9%, 174.2% and 187.5%, respectively (Table S5).

3.3. Auxin content of lettuce roots treated with different concentrations of CuO NP

LC-MS/MS results showed that the main component of auxin in lettuce root was indoleacetic acid (IAA), while other compontents such as Indole-3-acetyl-L-tryptophan (IAA-Trp), Indole-3-acetyl glycine (IAA-Gly) and 3-Indoleacrylic acid (IA) were not detected in the test. As shown in Table 2, there was no significant change in IAA concentration under 5 mg L^{-1} CuO NP, but the concentration of IAA decreased significantly from 20.3 ng g^{-1} to 11.4 ng g^{-1} at high concentration CuO NP.

3.4. Endodermal appolastic barriers development

TEM results showed that CuO NPs were mainly distributed in the cell wall, intercellular space and dead cells (especially in epidermal and cortical cells), and obvious Cu peaks were also detected in the corresponding EDS spectra (Fig. 2; Fig. S2). As shown in the Fig. 3B, continued PI uptake confirmed that the endodermal diffusion barrier was not formed under 5 mg L^{-1} CuO NPs treatment. However, the appolastic barrier was fully developed upon 450 mg L^{-1} CuO NPs exposure, which eventually blocked penetration of PI, leading to a strong delay in the block of PI uptake (block at 36.3 ± 0.4 cells) as well. Therefore, combined with the above results, 450 mg L^{-1} CuO NPs induced the accelerated appolastic barrier development and hindered the lateral transport of CuO NPs, for CuO NPs were surely not found in the endodermis cell of the elongated region via TEM-EDS (Fig. 2).

3.5. Root cell wall structure

Here, SEM-EDS (Fig. 2) and TEM (Fig. 4) analysis of different positions in root cross sections showed that there were many damaged cell walls in the epidermis, which may be caused by the attack of CuO NPs, suggesting that NPs could enter lettuce roots by impacting the cell wall. In addition, the ultrastructure of cells and the anatomical structure of root changed under different concentrations of CuO NPs. As shown in Fig. 4, under 5 mg L^{-1} CuO NPs treatment, the cells were arranged orderly and closely, and the thickness of the epidermal cell wall was much thinner than that of CK. Although the thickness of the cortical cells did not change, the intercellular space was larger and increased by 45.4% compared with that of CK. In contrast, the thickness of the cell wall in the cortex and endodermis increased from 0.21 μm to 0.45 μm with 450 mg L^{-1} CuO NPs exposure. Meanwhile, the contents of cellulose and lignin increased by 28.7% and 52.9% respectively (Fig. 6). Through immuno-TEM (Fig. 5D), we found that there were a large number of gold nanoparticle-labeled homogalacturonan in the narrow gap between cell walls. However, only a small amount of labeled homogalacturonan was detected in the intercellular space when treated

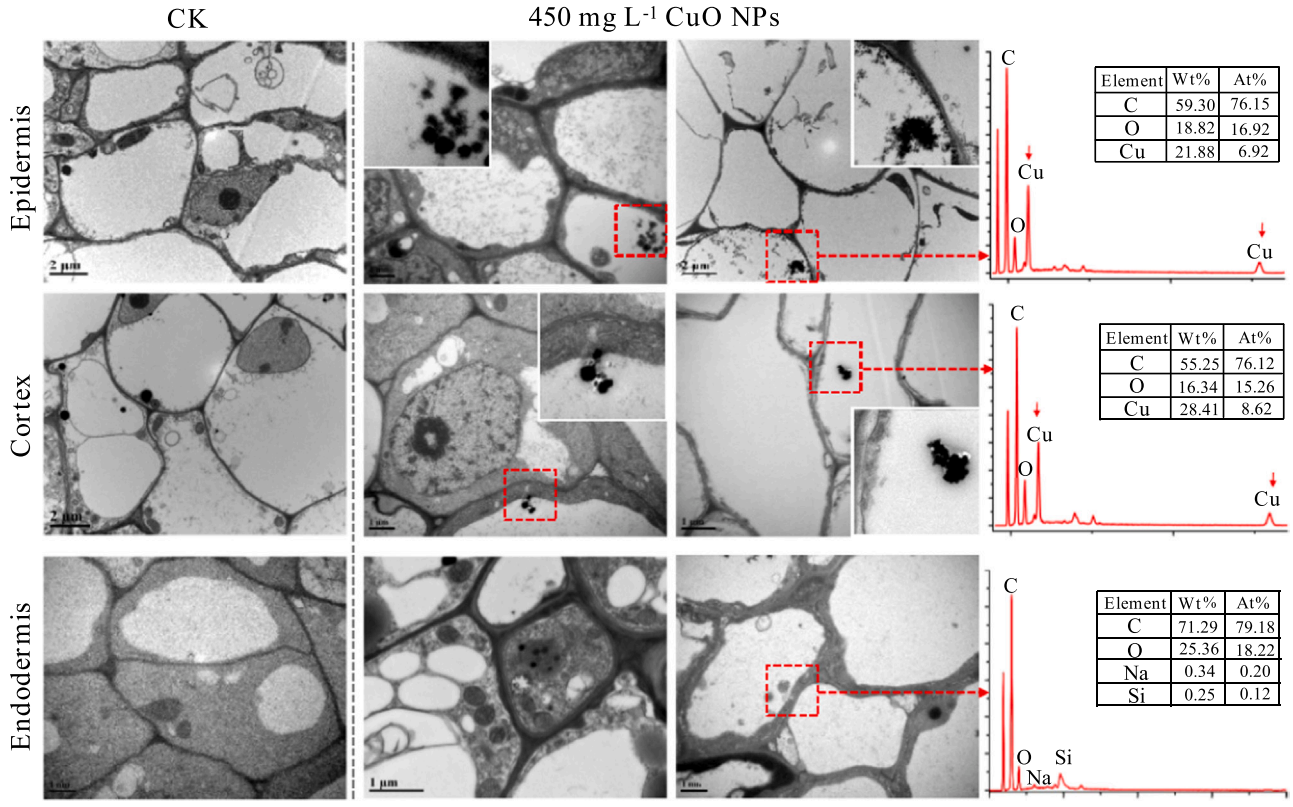

Fig. 2. The location of CuO NPs in 7-day-treated lettuce roots (epidermis, cortex and endodermis) is detected by TEM and SEM-EDS analysis, samples without CuO NPs treatment were used as control (CK, the first column). In order to fully reflect the accumulation of nanoparticles in the root, we provide root transverse sections at different sampling positions. The section sampling point in the second column is far away from the root cap, while the section sampling point in the third column is close to the root cap where most of cells are empty (dead).

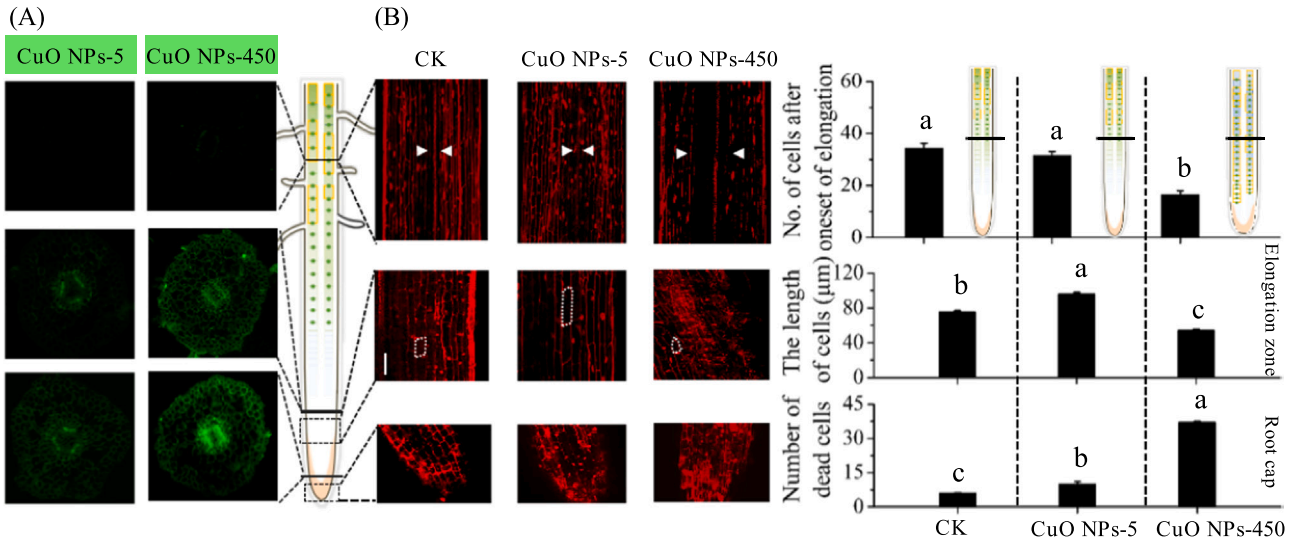

Fig. 3. (A) Cu fluorescence localization using Cu^{2+} probe in root cross-sections of lettuce with different levels of CuO NPs supply. (B) Anatomical analysis of various root segments in lettuce exposed to different concentrations of CuO NPs. It includes the number of dead cells of root cap and the length of elongation zone cells, as well as the development of apoplastic barriers which were quantified by PI and the number of endodermis cells after elongation by permeation of PI for 5 min (apoplastic barriers formation were shown by schematic diagrams). Scale bars: 3 cm. The white arrows represent the penetration of PI into stele and the white circles represent the outline of cell wall. Error bars are ± SD ($n = 4$).

with 5 mg L^{-1} CuO NPs.

3.6. Polysaccharides modification

The FTIR spectra (Fig. S6) suggested that hemicellulose 1 and pectin have rich functional groups, such as carbohydrate C-OH (1100–1000 cm^{-1}) and carboxylate radicals (1426–1420 cm^{-1}), which endowed RCW with a strong binding capacity to CuO NPs. Under 450 mg L^{-1} CuO NPs treatment, hemicellulose 1, 2 and pectin contents increased by 29.3%, 41.8% and 18.8% respectively from control levels, whereas the degree of methylation of pectin decreased compared with CK (Figs. 5B, C and 6). Although the content of the main neutral monosaccharides (including glucose, rhamnose and galactose) in pectin did not change significantly (Table 1), the concentration of glucuronic acid decreased with 5 mg L^{-1} CuO NPs exposure. However, when the inhibition rate was over 40%, the fluorescence intensity of LM19 (homogalacturonan monoclonal antibody, Verhertbruggen et al., 2009, Fig. 5A) became weak and unevenly distributed, but there was a strong fluorescence signal in the intercellular space. As shown in Fig. 1C, hemicellulose is the main binding site of CuO NPs on the lettuce cell wall and GC-MS analysis showed that xylose and glucose were the main monosaccharides of RCW hemicellulose (Table 1). Interestingly, the monosaccharide content and composition of hemicellulose 1 and 2 did not change significantly under low concentration of CuO NPs (Table S5), but the activities of two enzymes related to xyloglucan modification, xyloglucan endohydrolase (XEH) and xyloglucan endotransglycosylase (XET), increased significantly ($P < 0.05$, Fig. 7A). Here, with 450 mg L^{-1} CuO NPs treatment, xyloglucan contents were significantly increased ($P < 0.05$), but XTH activities were inhibited by more than 20%.

3.7. mRNA expression level of cell-wall-remodeling genes

Galacturonosyltransferase 1 (*GAUT1*) is a galacturonosyltransferase that transfers galacturonic acid to the pectic polysaccharide homogalacturonan (Atmodjo et al., 2011). Here, the expression of *GAUT1* was inhibited with a low concentration of CuO NPs but increased under high concentrations, which was consistent with the increased pectin concentrations. Compared with CK, the activity of PME was more than doubled under the action of high concentration nanoparticles, however, there was no significant change under low concentration (5 mg L^{-1}) treatment. Notably, 450 mg mL^{-1} CuO NPs treatment had a positive effect on the expression of *PME3* whereas the expression of *PME17* was not changed by CuO NPs supply. Consistent with the reduced expression levels of *XTH15*, *XTH17* and *XTH31*, the action of XET and XEH was remarkably inhibited under high concentrations (450 mg L^{-1}) of CuO NP stress (Fig. 7).

4. Discussion

At present, there is no unified conclusion on whether the phytotoxicity of NPs to plants comes from themselves or the released metal cations, which is related to their properties and the interaction between plants and NPs (Miralles et al., 2012; Verma et al., 2018; Milewska-Hendel et al., 2021). Considering that the charge and stability of NPs will define their absorption within plants (Milewska-Hendel et al., 2017, 2019), we first measured the surface charge of CuO NPs and their stability in nutrient solution. The results showed that the charge of CuO NPs in nutrient solution was mostly negative, and the absolute value of zeta potential sequentially increased with increasing exposure concentration (Table S3). The concentration of Cu^{2+} released by different concentrations of CuO NPs was time dependent, reaching a concentration of 0.62–2.54 mg L^{-1} after 72 h (pH 5.85, Fig. S3). Moreover, compared with the treatments receiving the same concentration of CuO bulk-particles (CuO BPs) and Cu^{2+} (which is equal to the concentration of Cu^{2+} released from CuO NPs), CuO NPs were the most toxic in both growth inhibition and the biomass decrease of roots and shoots (Fig. S4). Margenot et al. (2018) found that CuO NPs produced dose-dependent increases in root diameter for carrot seedlings, and the adverse effects of CuO NPs on root physiology are not necessarily attributed to Cu^{2+} toxicity. Consistently, our results provided evidence that the phytotoxicity of CuO NPs essentially resulted from the unique property of CuO NPs themselves.

4.1. Low concentration CuO NPs promoted lettuce root elongation by RCW loosening

Root elongation is a basic index that can be used to evaluate the phytotoxicity of pollutants such as nanoparticles (Kopittke and Wang, 2017). For example, wheat root length was reduced by 60% from control

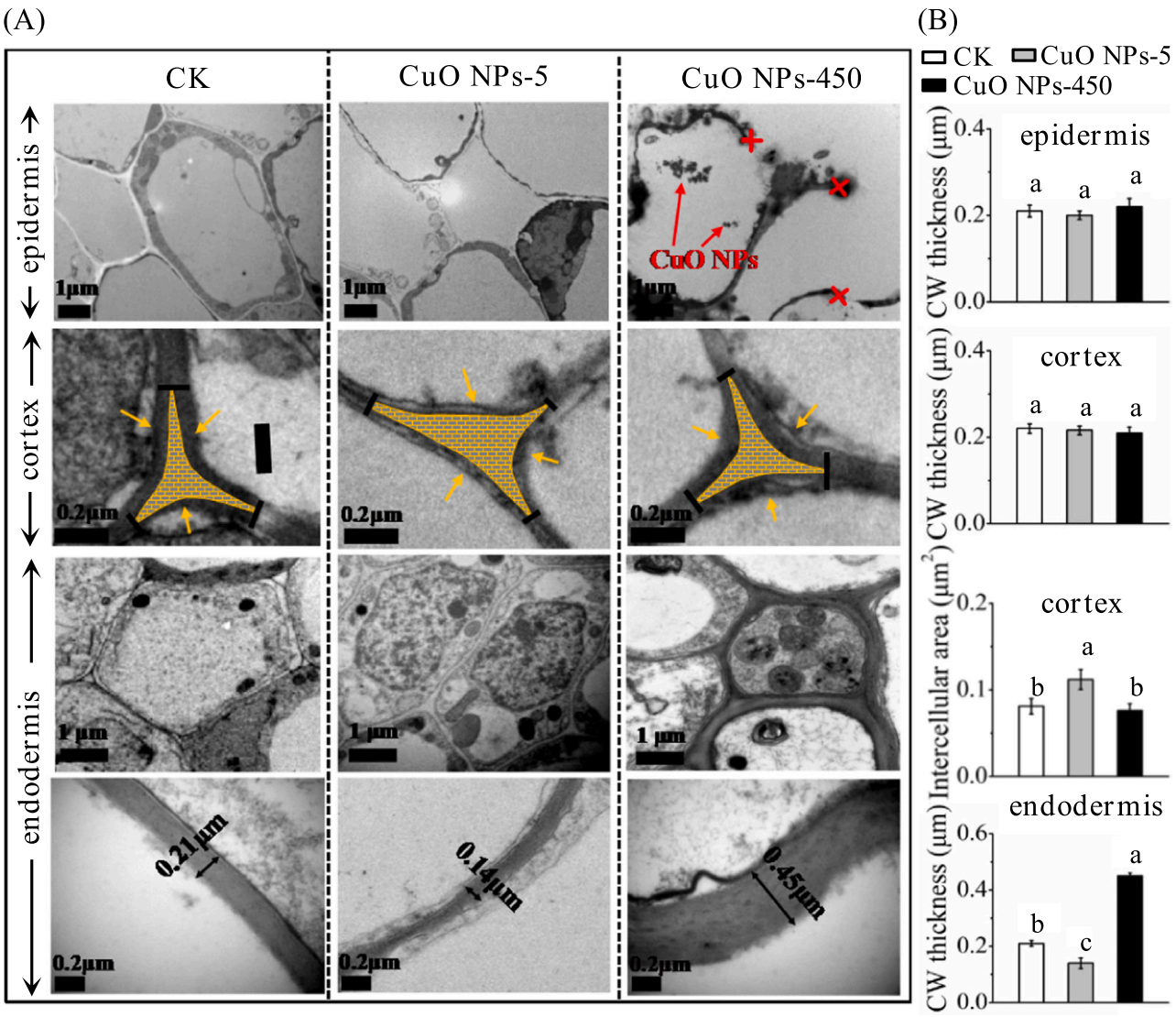

Fig. 4. Effects of different treatments on cell wall structure of lettuce roots. (A) TEM spectra of different positions among roots cross-sections, yellow cross marks the attack site of CuO NPs on cell wall, and the yellow grids represent the intercellular space between endodermis cells. (B) The thickness of RCW and the area of intercellular space between cortex cells were quantified by ImageJ. After the 7-day-supply with 0, 5 mg L^{-1} and 450 mg L^{-1} CuO NPs, the plants were harvested and the root segments (in the distance of 0.5–0.8 mm from root tips) were measured. The length represented by the scale bar has been identified in the figure. Values represents means ± SD ($n = 4$) and different letters indicate significant differences ($P < 0.05$) among the treatments.

levels under ZnO NPs (500 mg metal [M] kg^{-1} sand) treatment (Dimkpa et al., 2013), and the dry weight of rapeseed was largely reduced by more than 75% at concentrations of 500 mg L^{-1} ZnO NPs (Mousavi Kouhi et al., 2014). Different from the above mentioned results, we found that CuO NPs led to dose dependent effects on the growth of lettuce roots (Fig. 1A, B), and 5 mg L^{-1} CuO NPs promoted lettuce root elongation by over 20%. Recent studies concerning the phytotoxicity of nanoparticles suggested that root elongation resulted from cell wall loosening, which was related to the enhanced ROS production (Xie et al., 2020; Wang et al., 2020). Generally, the production and elimination of ROS in plants is basically in dynamic balance (Gapper and Dolan, 2006), but the steady state of redox state will be disrupted in the face of abiotic stress (Fry et al., 2002; Franková and Fry, 2013). For instance, Kim et al. (2014) reported that the exposure of nZVI to plants enhanced root elongation due to OH radial induced cell wall loosening. Consistently, low concentration of CuO NPs showed positive effects on lettuce roots, with the length of its elongation zone cells increasing by 28.2%. Meanwhile, compared to the CK treatment, the concentration of pectic glucuronic acid decreased by 17% under 5 mg L^{-1} CuO NPs (Fig. 6), and we speculated that the increased $OH^{\cdot}$ and $O_2^{\cdot -}$ would attack the pectic galacturonate residue and combine with its carboxyl group (Messenger et al., 2009). Besides, it was observed by immuno-TEM that low concentration of CuO NPs reduced the content of homogalacturonan in the intercellular space (Fig. 5D) between endodermis cells, resulting in the weaker adhesion of pectin and the looser cell wall compared with the CK treatment.

Notably, XET and XEH are two enzymes that can participate in the shear, reconnection and hydrolysis of xyloglucan, and the elongation rate of root cells may depend on the relative amounts of xyloglucan to XTH (Van Sandt et al., 2007; Zhu et al., 2012). Herein, XTH activities were induced, while xyloglucan content showed no significant change under 5 mg L^{-1} CuO NPs treatment. In this case, XTH could enter the cell wall in the form of free enzyme and shear xyloglucan to relax the cell wall structure, and finally promote cell elongation. Besides, root elongation is also associated with auxin transport (Blilou et al., 2005), and high IAA content may lead to cell wall remodeling and cell elongation (Xie et al., 2020). For example, auxin can affect hemicellulose, pectin and lignin levels (Schindler et al., 1995). Additionally, the effect of auxin

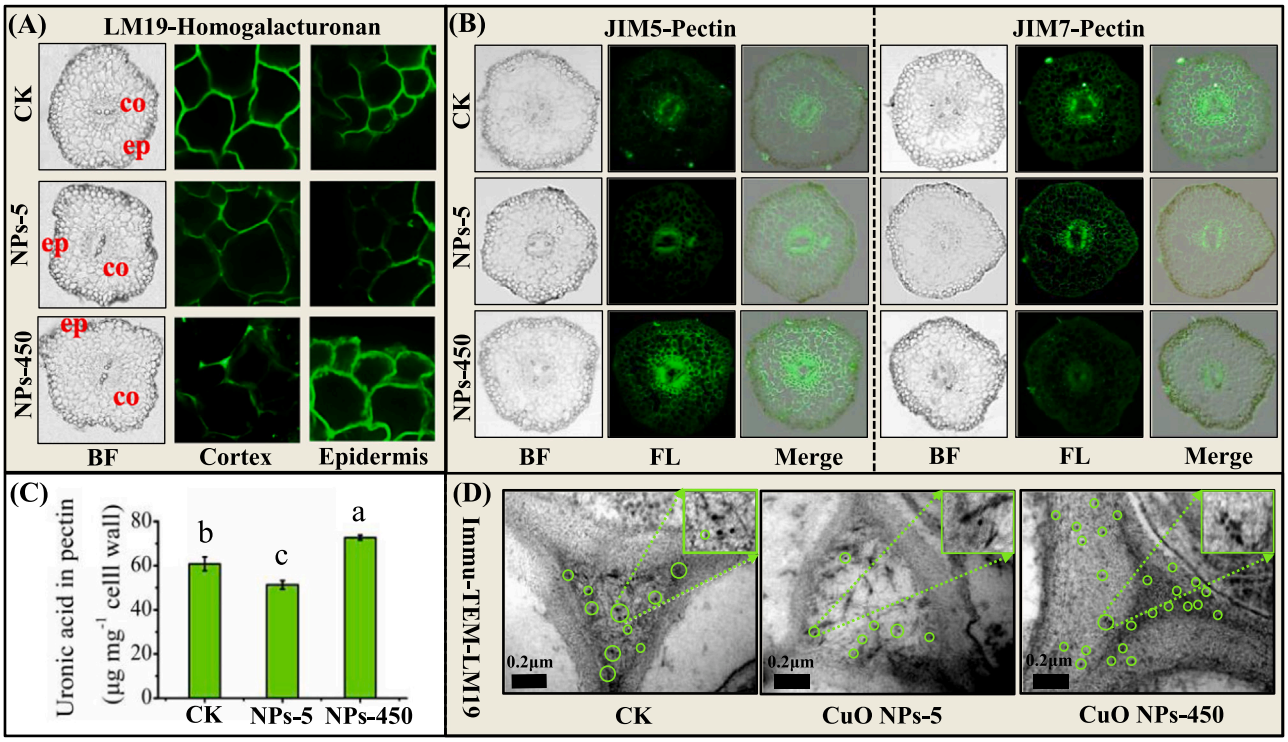

Fig. 5. Effects of different treatments on the composition and distribution of RCW pectin in lettuce roots. Immunolocalization of pectic homogalacturonan (LM19 epitope, A, mainly represented the root epidermis and cortex), low-methylesterified pectin (JIM5 epitope, B) and high-methylesterified pectin (JIM7 epitope, B) in root cross-sections of lettuce. The content of uronic acid (C) in RCW pectin and the immunolocalization of homogalacturonan in endodermis (D) were also detected. Plants were treated by nutrient solution without (CK) and with CuO NP s (5 mg L^{-1} and 450 mg L^{-1}) for 7 d. The green circles in graph (D) represent gold nanoparticles of homogalacturonan and scale bars are 0.2 mm. Values represents means ± SD ($n = 4$) and different letters indicate significant differences ($P < 0.05$) among the treatments. BF: bright field images; FL: fluorescence images; ep: epidermis; co: cortex.

on cell wall synthesis is linked to the "Acid growth theory" that auxin can cause cell wall relaxation by inserting H^+ into the cell wall via H^+-ATPasse (Nikonorova et al., 2021). Considering that IAA concentration did not increase significantly with the addition of 5 mg L^{-1} of CuO NP (Table 2), we could not determine the role of auxin on the growth of lettuce root in response to CuO NP from the existing data. The regulatory mechanism by which auxin affects root growth by inducing cell wall modification is worth exploring in the future.

4.2. *High concentration CuO NPs triggered RCW polysaccharide modification which inhibited lettuce root elongation*

It is well known that NPs can cause oxidative damage by attacking the antioxidant system of plants, for instance, AgNPs induced ROS accumulation in root tips of *A. thaliana*, especially enhanced the concentrations of $O_2^{\bullet-}$ and H_2O_2 (Wang et al., 2020). Here, 450 mg L^{-1} CuO NPs activated the antioxidant defense system and resisted the oxidative stress produced by ROS (Fig. 1D, E), however, it did not alleviate the oxidative stress in lettuce. For the fact is, there were a large number of dead cells appeared in the root tip, also the length and volume of epidermal cells in elongation zone were reduced (Fig. 3B). Thus, in contrast to 5 mg L^{-1} CuO NPs, 450 mg L^{-1} CuO NPs resulted in a 48.5% reduction in the root of lettuce at the end of the 7-day treatment (Fig. 1).

The majority of metal ions are bound to the RCW, which is an important mechanism for plants to cope with abiotic stress (Krzesłowska, 2011). Within complex cell wall components, pectin is an attractive polysaccharide that exposes a large number of binding sites under the regulation of pectin methylesterase (PME) and a series of PME encoding gene families (Lux et al., 2010; Xiao et al., 2020). However, the accumulation of CuO NPs and their released Cu^{2+} may replace the Ca^{2+} in the cell wall, and damage the "egg box model" of pectic homogalacturonan which plays an important role in stabilizing the RCW structure (Cosgrove, 2016), eventually hindering root elongation (Fry et al., 2002). Besides, previous studies confirmed that pectin modification was also involved in root growth (Xiao et al., 2021; Liu et al., 2021). For example, Li et al. (2009) suggested that the combination of Al and pectin prevented the adhesion of newly synthesized polysaccharides to the cell wall, resulting in disorganized distribution of pectin and thus inhibiting root elongation in maize. As we know that the intercellular layer is derived from the late mitotic cell plate which is rich in homogalacturonan (De Lorenzo et al., 2018), therefore, the disorder of homogalacturonan distribution caused by high concentration of CuO NPs may affect the process of intercellular separation and cell extension (Cosgrove, 2016). In addition, with 450 mg L^{-1} CuO NPs exposure, xyloglucan contents were significantly increased ($P < 0.05$), but XTH activities were inhibited by more than 20% (Figs. 6 and 7), therefore XTH could only use xyloglucan which had been bound to the cell wall as the receptor substrate. As a result, RCW became more compact and the cell elongation was inhibited.

4.3. *Root cell wall remodeling enhanced tolerance of lettuce to CuO NPs*

Previous studies confirmed that nanoparticles could enter the plant via the apoplast pathway because the resistance of the apoplastic space is relatively low (Rossi et al., 2017; Yue et al., 2019). However, some studies have indicated that the apoplastic barrier is also a protective mechanism in response to external stress, which can prevent metal ions and nanoparticles from entering plants (Lux et al., 2010; Lee et al., 2013). Furthermore, the position of appolastic barriers affects the transport of water and ions in plant roots (Yue et al., 2019), for example, CeO_2 NPs were found to accelerate the deposition of Casparian strips and suberin lamellae, which resulted in a large amount of Na^+ flowing into the root of *Brassica napus* (Rossi et al., 2017). Like that, does the development position of appolastic barriers affect the absorption of Cu^{2+}

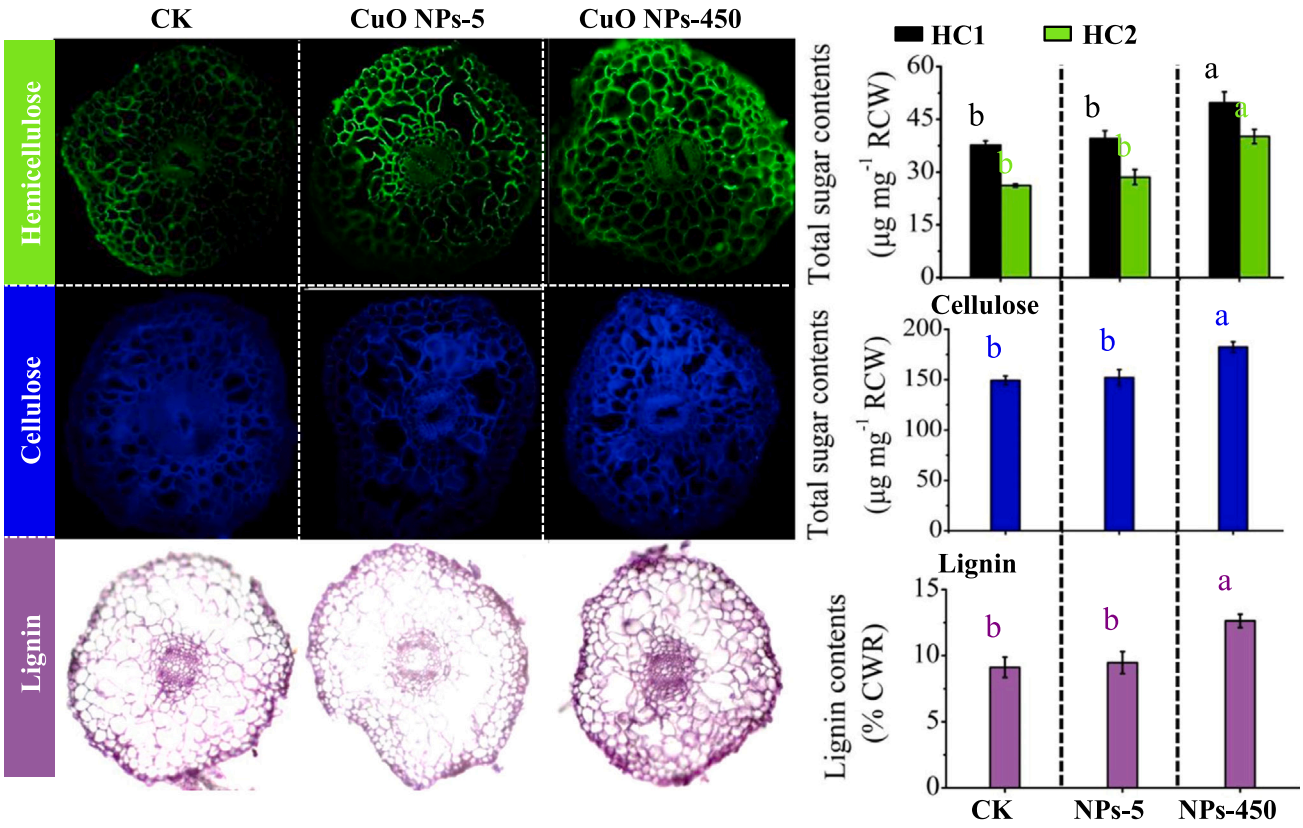

Fig. 6. Immunolocalization of xyloglucan (CRCCM99), and the light microscopy observation of cellulose in cross-sections of lettuce roots (in the distance of 0.5–0.8 mm from root tips) with different treatment for 7 d. Contents of hemicellulose 1 and 2, as well as cellulose were quantified by total sugar, and lignin content was calculated as a percentage of root CWR dry weight. Values represents means ± SD ($n = 4$) and different letters indicate significant differences ($P < 0.05$) among the treatments. HC1: hemicellulose 1; HC2: hemicellulose 2.

Table 1
Monosaccharide composition of pectin, hemicellulose 1 and 2 of lettuce exposed to CuO NPs for 7 d. The figures in brackets indicate the percentage of this monosaccharide accounts for the total polysaccharide. Data as means ± SD ($n = 3$).

Sample	Treatment	Monosaccharide composition (μmol g^{-1} dry cell wall)							
		Rha	Fuc	Ara	Xyl	Man	Glu	Gal	Total
Pectin	CK CuO NPs-5	1.31 ± 0.12	0.30 ± 0.02	0.31 ± 0.03	0.43 ± 0.03	1.01 ± 0.09	3.67 ± 0.18	2.32 ± 0.15	9.36 ± 0.87
		1.49 ± 0.15	0.09 ± 0.01	0.16 ± 0.01	0.19 ± 0.01	0.71 ± 0.05	3.76 ± 0.24	4.29 ± 0.35	10.69 ± 0.95
	CuO NPs-450	4.41 ± 0.23	0.11 ± 0.01	0.37 ± 0.02	0.42 ± 0.03	0.94 ± 0.08	5.97 ± 0.37	5.12 ± 0.41	17.33 ± 1.15
Hemicelloluse1	CK	0.52 ± 0.05	0.18 ± 0.01	2.25 ± 0.16	16.02 ± 0.95	0.64 ± 0.05	10.48 ± 0.93	1.26 ± 0.10	31.35 ± 1.76
	CuO NPs-5	0.34 ± 0.04	0.36 ± 0.02	1.82 ± 0.17	14.76 ± 0.75	1.01 ± 0.06	12.92 ± 1.02	0.71 ± 0.05	31.93 ± 1.58
	CuO NPs-450	0.46 ± 0.05	0.18 ± 0.01	3.11 ± 0.25	31.41 ± 1.73	1.13 ± 0.12	12.54 ± 1.14	2.15 ± 0.22	50.99 ± 3.16
Hemicelloluse2	CK	0.30 ± 0.03	0.24 ± 0.02	0.56 ± 0.05	7.74 ± 0.55	0.72 ± 0.05	1.81 ± 0.12	0.54 ± 0.03	11.92 ± 1.02
	CuO NPs-5	0.20 ± 0.01	0.14 ± 0.01	0.91 ± 0.07	6.88 ± 0.64	0.83 ± 0.06	1.35 ± 0.10	0.30 ± 0.02	10.60 ± 0.96
	CuO NPs-450	0.58 ± 0.03	0.31 ± 0.02	0.54 ± 0.05	12.30 ± 0.92	1.29 ± 0.09	1.72 ± 0.15	0.58 ± 0.05	17.33 ± 1.54

Rha: rhamnose; Fuc: fucose; Ara: arabinose; Xyl: xylose; Man: mannose; Glu: glucose; Gal: galactose

in roots? By in situ observation with a Cu^{2+} probe (Zhang et al., 2014), we found that the fluorescence signal of Cu^{2+} could still be detected in the area above the root tip (approximately 50 mm away from root tips) with low concentration of CuO NPs. Nevertheless, upon exposure to 450 mg L^{-1} CuO NPs, Cu hardly be detected in this area, but there was a very strong Cu aggregation in the root tip (Fig. 3A). This further indicated that the formation of appolastic barriers was more advanced under the treatment of high concentration of CuO NPs, resulting in a large number of CuO NPs and Cu^{2+} could only be gathered in the root tip, but unable to be transported in the above area where the appolastic barrier was fully developed. In addition, some studies have reported that nanoparticles affect the development of root hairs and enter plants through lateral roots (Verma et al., 2018; Milewska-Hendel et al., 2019). For example, Peng et al. (2015) suggested that the formation of lateral root may provide a possible pathway for CuO NPs to enter the stele in *Oryza sativa*. Considering that there is controversy about the uptake of nanoparticles by plants, more research needs to be carried out to clarify translocation and stress modulation mechanisms of nanoparticles in plants, especially in areas above the root tip.

Based on the fluorescence microscope, we clearly noted that a large number of CuO NPs were gathered around roots (Fig. S1A), but could they be absorbed by the plant root and then transported to the xylem? Lin and Xing (2008) found the presence of ZnO NPs in the endodermis and vascular bundle cells, which indicated that ZnO NPs could enter into the root cells by creating cell wall pores and increasing the permeability of the cell wall. Similarly, a large number of CuO NPs were observed in the cell wall of epidermal and cortical cells, but no Cu signal was detected in endodermis (Fig. 3B), indicating that CuO NPs could be

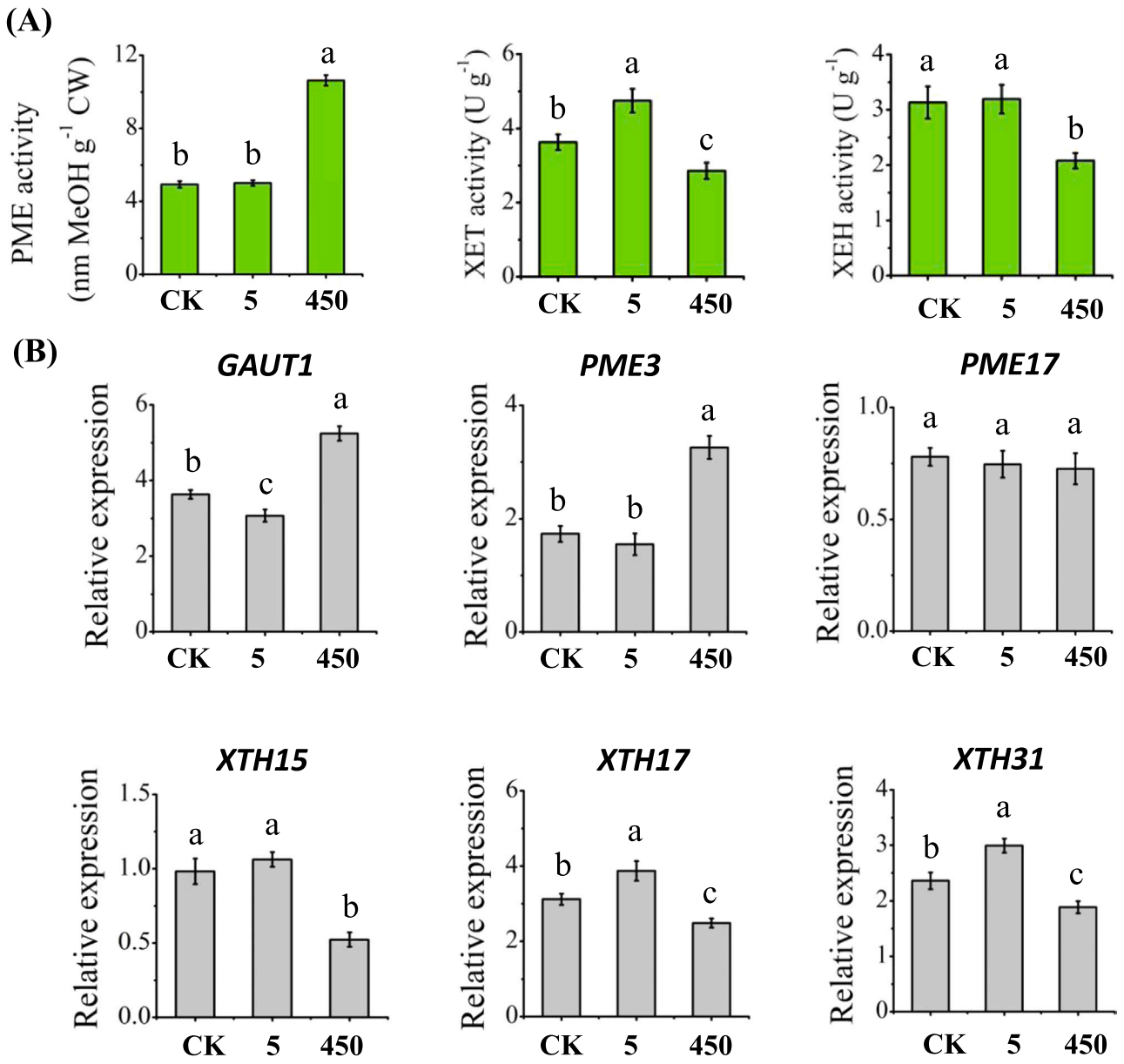

Fig. 7. Changes of pectin methylesterase (PME), xyloglucan endotransglycosylase (XET) and xyloglucan endohydrolase (XEH) activities of lettuce roots under different treatments (A), as well as the quantitative PCR analysis (B) of the expression of genes (*GAUT1*, *PME3*, *PME17*, *XTH15*, *XTH17* and *XTH31*) related to cell wall synthesis in lettuce roots with different levels of CuO NPs for 7 d. Values represents means ± SD ($n = 4$) and different letters indicate significant differences ($P < 0.05$) among the treatments. Names of genes have been labeled on their own graphs. The terms 5 and 450 in graphs represent 5 mg L^{-1} and 450 mg L^{-1} CuO NPs, respectively.

absorbed by lettuce roots, but their migration would be hindered to xylem. Due to the toxicity of high concentration CuO NPs, most epidermal and cortical cells lack cytoplasmic matrix, and the cell wall becomes deformed and empty (Fig. S2). Meanwhile, compared with CK, the thickness of endothermic cell wall was significantly thickened under 450 mg L^{-1} CuO NPs compared with CK treatment (Fig. 4). In general, thickened RCW are specialized and lignified cell wall structures, with cellulose microfibrils comprising the majority of thickenings (Aleamotu et al., 2019; Kang et al., 2019). Previous studies suggested that exposure to CuO NPs induced the modification of root architecture and enhanced lignification in roots of *Brassica* plants (Nair and Chung, 2015; Wang et al., 2020). Herein 450 mg L^{-1} CuO NPs increased the content of cellulose and lignin (Fig. 6), thus leading to the enhanced cell wall fixation and the blocking of ion transport, which could reduce the toxicity of CuO NPs to protoplasts.

In general, plant response to abiotic stress is a process that required diverse enzymatic reactions related to cell wall metabolism, and is regulated by encoding genes responsible for cell wall remodeling (Cosgrove, 2016; Xiao et al., 2020). For example, transcriptome analysis suggested that pectin biosynthesis was one of the key processes involved in Cd accumulation, and most GAUT related unigenes had higher expression levels in a low-Cd-accumulating cultivar of water spinach (*Ipomoea aquatic* Forsk.) (Huang et al., 2016). Similarly, the anti-Cd toxicity mechanism of *Tor-1* involved gene regulation (*PME17*) to increase pectin concentrations and PME activities, thereby reducing Cd toxicity in cellular organelles of *Arabidopsis thaliana* (Sénéchal et al., 2014). In contrast to the above results, the expression of *PME17* did not change with CuO NPs exposure compared with CK treatment, whereas the expression of *PME3* was significantly upregulated with 450 mg mL^{-1} CuO NPs addition, which was consistent with the increased PME activities. The above changes exposed a large number of binding sites to hold more Cu and CuO NPs on RCW and avoid damage to protoplasts, as

Table 2
Auxin content in root of lettuce under different treatments. Data as means ± SD ($n = 3$).

Index concentration (ng g^{-1})	CK	5 mg L^{-1} CuO NP	450 mg L^{-1} CuO NP
IAA	20.3 ± 0.98	20.9 ± 0.82	11.4 ± 0.77
IAA-Trp	N/A	N/A	N/A
IAA-Phe	N/A	N/A	N/A
IAA-Gly	N/A	N/A	N/A
IAA-Glu	N/A	N/A	N/A
IAA-Glc	N/A	N/A	N/A
IAA-Leu-Me	N/A	N/A	N/A
IA	N/A	N/A	N/A

IAA: Indole-3-acetic acid; IAA-Trp: Indole-3-acetyl-L-tryptophan; IAA-Phe: N-(3-Indolylacetyl)-Lphenylalanine; IAA-Gly: Indole-3-acetyl glycine; IAA-Glu: Indoleacetyl glutamic acid; IAA-Glc: 1-O-indol-3-ylacetylglucose; IAA-Leu-Me: Indole-3-acetyl-L-leucine methylester; IA: 3-Indoleacrylic acid. N/A means not available in this test.

similar phenomenon can be observed in *Brassica napus* against ZnO NPs (Molnár et al., 2020). Besides, xyloglucosan endogenous transglycosylase and hydrolases, regulated by *XTH* genes (Park and Cosgrove, 2012), are considered to be involved in reduced metal toxicity and root growth. Here, has the CuO NPs exposure concentration increased, the activity of XET and the down expression levels of *XTH15* and *XTH31* decreased significantly (Fig. 7). Interestingly, the expression of *XTH17* and *XTH31* was consistent, representing an increase at low concentrations but a decrease at high concentrations of CuO NPs, further indicating that the two genes existed as dimers to participate in RCW modification (Zhu et al., 2014; Guo et al., 2020), and affected root elongation in lettuce.

Taken together, our results demonstrated that the opposite effects of different concentrations of CuO NPs on lettuce roots were associated with RCW remodeling which can be summarized in Fig. 8. In the pursuit of sustainable applications of nanotechnology and safe agriculture, more work is needed to characterize the toxicity and accumulation of NPs in plants to ensure the safe application of nanoparticles in agricultural strategies.

5. Conclusion

CuO NPs changed the composition and structure of RCW and ultimately affected the growth of lettuce roots. Exposure to 5 mg L^{-1} CuO NPs promoted the production of ROS within roots and triggered a series

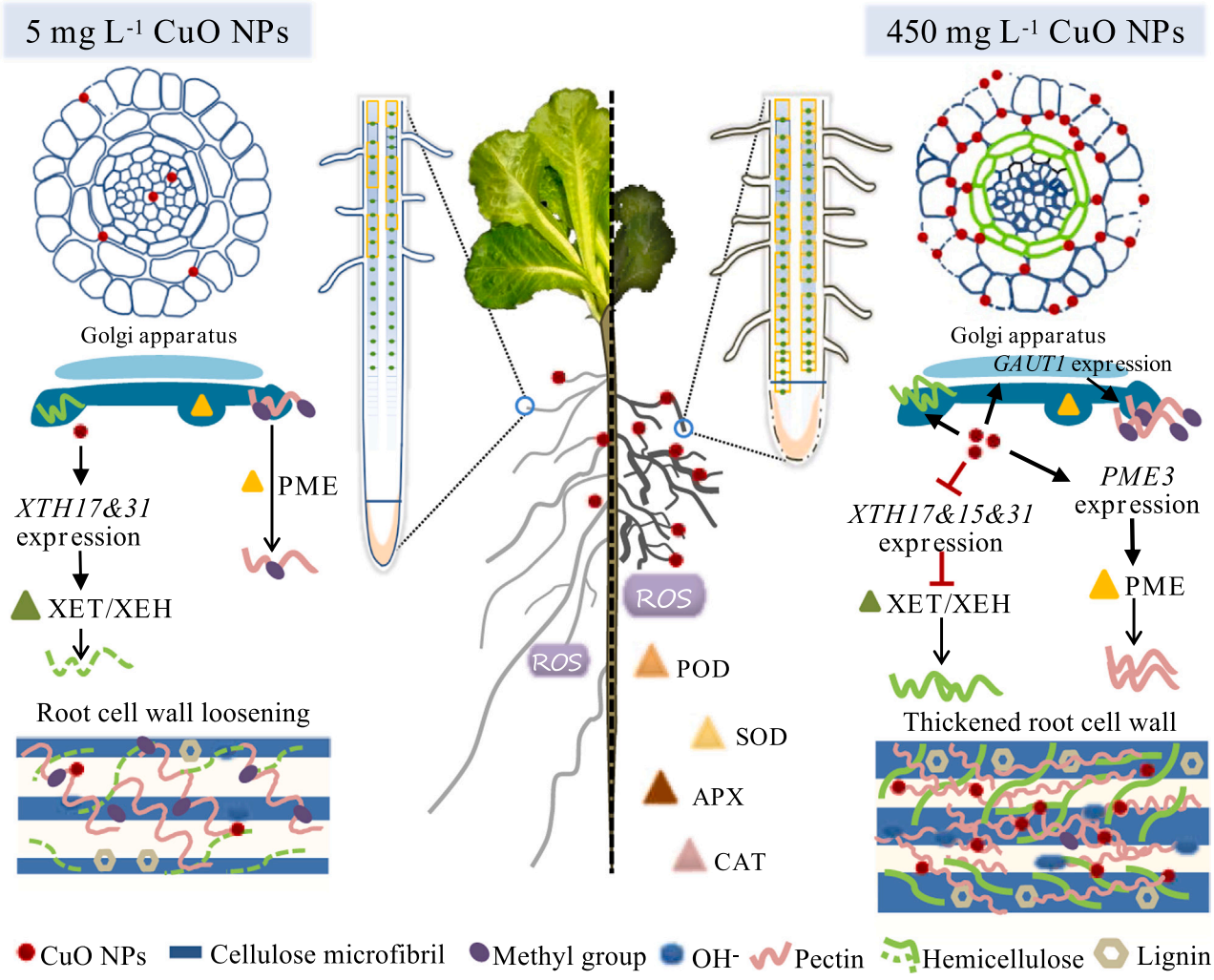

Fig. 8. Summary of the role of RCW remodeling in lettuce exposed to CuO NPs. 5 mg L^{-1} CuO NPs enhanced root elongation by inducing cell wall loosening, however, 450 mg L^{-1} CuO NPs triggered RCW polysaccharide modifications which made roots difficult to extend, roots became thick and short. The thickness of RCW was opposite under different concentrations of CuO NPs, and further investigations suggested that regulation of some key genes related to RCW remodeling participated in the impacts of CuO NPs on the lettuce root growth. PME: pectin methylesterase; XET: xyloglucan endotransglycosylase; XEH: xyloglucan endohydrolase; ROS: reactive oxygen species; POD: peroxidase; SOD: superoxide dismutase; APX: ascorbate peroxidase; CAT: catalase.

of RCW polysaccharide modifications, thus inducing notable cell wall loosening. However, under 450 mg L^{-1} CuO NPs treatment, the disordered distribution of pectic homogalacturonan and the various relative amounts of xyloglucan and XET/XEH made RCW stiffening and difficult to extend. In addition, the development of apoplastic barrier, increased lignin and low-methylesterified pectin, as well as the thickened RCW structure collectively enhanced the resistance of lettuce to CuO NPs. Our study revealed the molecular mechanisms underpinning RCW remodeling of lettuce in response to CuO NPs, providing a step forward for understanding the causes of NPs phytotoxicity in plants.

CRediT authorship contribution statement

Xinyu Guo: Investigation, Data curation, Writing – original draft. **Jipeng Luo:** Data curation, Writing – review & editing. **Ran Zhang:** Investigation, Data curation. **Hairong Gao:** Investigation, Data curation. **Liangcai Peng:** Methodology, Writing – review & editing. **Yongchao Liang:** Writing – review & editing. **Ting qiang Li:** Methodology, Writing – review & editing, Supervision.

Declaration of Competing Interest

The authors declare that they have no known competing financial interests or personal relationships that could have appeared to influence the work reported in this paper.

Acknowledgments

This research was financially supported by Zhejiang Provincial Natural Science Foundation of China (LZ18D010001), the National Natural Science Foundation of China (41671315, 41977107) and the Fundamental Research Funds for the Central Universities (2020FZZX001-06).

Author agreement

All authors have read and approved the manuscript.

Author contributions

X.Y.G., J.P.L, Y.C.L. and T.Q.L. designed the research, X.Y.G., J.P.L, R.Z., H.R.G. and L.C.P. performed the research, X.Y.G., R.Z. and H.R.G. analyzed the data, X.Y.G., and T.Q.L. wrote the article.

Appendix A. Supporting information

Supplementary data associated with this article can be found in the online version at doi:10.1016/j.envexpbot.2022.104906.

References

Adams, J., Wright, M., Wagner, H., Valiente, J., Britt, D., Anderson, A., 2017. Cu from dissolution of CuO nanoparticles signals changes in root morphology. Plant Physiol. Biochem. 110, 108–117.

Alassimone, J., Naseer, S., Geldner, N., 2010. A developmental framework for endodermal differentiation and polarity. Proc. Natl. Acad. Sci. USA 107, 5214–5219.

Aleamotu M., A., McCurdy, D.W., Collings, D.A., 2019. Phi thickenings in roots: novel secondary wall structures responsive to biotic and abiotic stresses. J. Exp. Bot. 70, 4631–4642.

Atmodjo, M.A., Sakuragi, Y., Zhu, X., Burrell, A.J., Mohanty, S.S., Atwood, J.A., Orlando, R., Scheller, H.V., Mohnen, D., 2011. Galacturonosyltransferase (GAUT)1 and GAUT7 are the core of a plant cell wall pectin biosynthetic homogalacturonan: galacturonosyltransferase complex. Proc. Natl. Acad. Sci. USA 108, 20225–20230.

Barberon, M., Vermeer, J.E.M., De Bellis, D., Wang, P., Naseer, S., Andersen, T.G., Humbel, B.M., Nawrath, C., Takano, J., Salt, D.E., Geldner, N., 2016. Adaptation of root function by nutrient-induced plasticity of endodermal differentiation. Cell 164, 447–459.

Blilou, I., Xu, J., Wildwater, M., Willemsen, V., Paponov, I., Friml, J., Heidstra, R., Aida, M., Palme, K., Scheres, B., 2005. The PIN auxin efflux facilitator network controls growth and patterning in *Arabidopsis* roots. Nature 433, 39–44.

Blumenkrantz, N., Asboe-Hansen, G., 1973. New method for quantitative determination of uronic acids. Anal. Biochem 54, 484–489.

Cosgrove, D.J., 2016. Plant cell wall extensibility: connecting plant cell growth with cell wall structure, mechanics, and the action of wall-modifying enzymes. J. Exp. Bot. 67, 463–476.

De Lorenzo, G., Ferrari, S., Giovannoni, M., Mattei, B., Cervone, F., 2018. Cell wall traits that influence plant development, immunity and bioconversion. Plant J. 97, 134–147.

Deng, C., Wang, Y., Cota-Ruiz, K., Reyes, A., Sun, Y., Peralta-Videa, J., Hernandez-Viezcas, J.A., Turley, R.S., Niu, G., Li, C., Gardea-Torresdey, J., 2020. Bok choy (*Brassica rapa*) grown in copper oxide nanoparticles-amended soils exhibits toxicity in a phenotype-dependent manner: Translocation, biodistribution and nutritional disturbance. J. Hazard. Mater. 398, 122978.

Dimkpa, C.O., Latta, D.E., McLean, J.E., Britt, D.W., Boyanov, M.I., Anderson, A.J., 2013. Fate of CuO and ZnO Nano- and microparticles in the plant environment. Environ. Sci. Technol. 47, 4734–4742.

Dubois, M., Gilles, K.A., Hamilton, J.K., Rebers, P.A., Smith, F., 1956. Colorimetric method for determination of sugars and related substances. Anal. Chem. 28, 350–356.

Franková, L., Fry, S.C., 2013. Biochemistry and physiological roles of enzymes that 'cut and paste' plant cell-wall polysaccharides. J. Exp. Bot. 64, 3519–3550.

Fry, S.C., Miller, J.G., Dumville, J.C., 2002. A proposed role for copper ions in cell wall loosening. Plant Soil 247, 57–67.

Gapper, C., Dolan, L., 2006. Control of plant development by reactive oxygen species. Plant Physiol. 141, 341–345.

Gomez, A., Narayan, M., Zhao, L., Jia, X., Bernal, R.A., Lopez-Moreno, M.L., Peralta-Videa, J.R., 2021. Effects of nano-enabled agricultural strategies on food quality: Current knowledge and future research needs. J. Hazard. Mater. 401, 123385.

Guo, X., Luo, J., Du, Y., Li, J., Liu, Y., Liang, Y., Li, T., 2021. Coordination between root cell wall thickening and pectin modification is involved in cadmium accumulation in *Sedum alfredii*. Environ. Pollut. 268, 115665.

Guo, X., Liu, Y., Zhang, R., Luo, J., Song, Y., Li, J., Wu, K., Peng, L., Liu, Y., Du, Y., Liang, Y., Li, T., 2020. Hemicellulose modification promotes cadmium hyperaccumulation by decreasing its retention on roots in *Sedum alfredii*. Plant Soil 447, 241–255.

Guo, X., Zhang, S., Luo, J., Pan, M., Du, Y., Liang, Y., Li, T., 2022. Integrated glycolysis and pyrolysis process for multiple utilization and cadmium collection of hyperaccumulator *Sedum alfredii*. J. Hazard. Mater. 422, 126859.

Huang, Y., Shen, C., Chen, J., He, C., Zhou, Q., Tan, X., Yuan, J., Yang, Z., 2016. Comparative transcriptome analysis of two *Ipomoea aquatica* Forsk. cultivars targeted to explore possible mechanism of genotype-dependent accumulation of cadmium. J. Agric. Food Chem. 64, 5241–5250.

Jain, A., Sinilal, B., Starnes, D.L., Sanagala, R., Krishnamurthy, S., Sahi, S.V., 2014. Role of Fe-responsive genes in bioreduction and transport of ionic gold to roots of *Arabidopsis thaliana* during synthesis of gold nanoparticles. Plant Physiol. Bioch. 84, 189–196.

Jones, D.L., Blancaflor, E.B., Kochian, L.V., Gilroy, S., 2006. Spatial coordination of aluminium uptake, production of reactive oxygen species, callose production and wall rigidification in maize roots. Plant Cell Environ. 29, 1309–1318.

Kang, X., Kirui, A., Dickwella, W.M., Mentink-Vigier, F., Cosgrove, D.J., Wang, T., 2019. Lignin-polysaccharide interactions in plant secondary cell walls revealed by solid-state NMR. Nat. Commun. 10, 347.

Kazan, K., 2013. Auxin and the integration of environmental signals into plant root development. Ann. Bot. 112, 1655–1665.

Kim, J., Lee, Y., Kim, E., Gu, S., Sohn, E.J., Seo, Y.S., An, H.J., Chang, Y., 2014. Exposure of iron nanoparticles to *Arabidopsis thaliana* enhances root elongation by triggering cell wall loosening. Environ. Sci. Technol. 48, 3477–3485.

Kopittke, P.M., Asher, C.J., Blamey, F.P.C., Menzies, N.W., 2009. Toxic effects of Cu^{2+} on growth, nutrition, root morphology, and distribution of Cu in roots of Sabi grass. Sci. Total Environ. 407, 4616–4621.

Kopittke, P.M., Wang, P., 2017. Kinetics of metal toxicity in plant roots and its effects on root morphology. Plant Soil 419, 269–279.

Kováč, J., Lux, A., Vaculík, M., 2018. Formation of a subero-lignified apical deposit in root tip of radish (*Raphanus sativus*) as a response to copper stress. Ann. Bot. 122, 823–831.

Krzesłowska, M., 2011. The cell wall in plant cell response to trace metals: polysaccharide remodeling and its role in defense strategy. Acta Physiol. Plant 33, 35–51.

Krzesłowska, M., Rabęda, I., Basińska, A., Lewandowski, M., Mellerowicz, E.J., Napieralska, A., Samardakiewicz, S., Woźny, A., 2016. Pectinous cell wall thickenings formation—a common defense strategy of plants to cope with Pb. Environ. Pollut. 214, 354–361.

Kurepa, J., Paunesku, T., Vogt, S., Arora, H., Rabatic, B.M., Lu, J., Wanzer, M.B., Woloschak, G.E., Smalle, J.A., 2010. Uptake and distribution of ultrasmall anatase TiO_2 alizarin red s nanoconjugates in *Arabidopsis thaliana*. Nano Lett. 10, 2296–2302.

Lee, Y., Rubio, M.C., Alassimone, J., Geldner, N., 2013. A mechanism for localized lignin deposition in the endodermis. Cell 153, 402–412.

Lenaghan, S.C., Li, Y., Zhang, H., Burris, J.N., Stewart, C.N., Parker, L.E., Zhang, M., 2013. Monitoring the environmental impact of TiO_2 nanoparticles using a plant-based sensor network. IEEE T Nanotechnol. 12, 182–189.

Lin, D., Xing, B., 2008. Root uptake and phytotoxicity of ZnO nanoparticles. Environ. Sci. Technol. 42, 5580–5585.

Liu, C., Chang, C., Fei, Y., Li, F., Wang, Q., Zhai, G., Lei, J., 2018. Cadmium accumulation in edible flowering cabbages in the Pearl River Delta, China: Critical soil factors and enrichment models. Environ. Pollut. 233, 880–888.

Liu, Y., Wu, R., Wan, Q., Xie, G., Bi, Y., 2007. Glucose-6-phosphate dehydrogenase plays a pivotal role in nitric oxide-involved defense against oxidative stress under salt stress in red kidney bean roots. Plant Cell Physiol. 48, 511–522.
Li, T., Tao, Q., Shohag, M.J.I., Yang, X., Sparks, D.L., Liang, Y., 2015. Root cell wall polysaccharides are involved in cadmium hyperaccumulation in *Sedum alfredii*. Plant Soil 389, 387–399.
Liu, X., Cui, H., Zhang, B., Song, M., Chen, S., Xiao, C., Tang, Y., Liesche, J., 2021. Reduced pectin content of cell walls prevents stress-induced root cell elongation in *Arabidopsis*. J. Exp. Bot. 72, 1073–1084.
Li, Y.Y., Yang, J.L., Zhang, Y.J., Zheng, S.J., 2009. Disorganized distribution of homogalacturonan epitopes in cell walls as one possible mechanism for aluminium-induced root growth inhibition in maize. Ann. Bot. 104, 235–241.
Lux, A., Martinka, M., Vaculik, M., White, P.J., 2010. Root responses to cadmium in the rhizosphere: a review. J. Exp. Bot. 62, 21–37.
Margenot, A.J., Rippner, D.A., Dumlao, M.R., Nezami, S., Green, P.G., Parikh, S.J., McElrone, A.J., 2018. Copper oxide nanoparticle effects on root growth and hydraulic conductivity of two vegetable crops. Plant Soil 431, 333–345.
Messenger, D.J., Mcleod, A.R., Fry, S.C., 2009. The role of ultraviolet radiation, photosensitizers, reactive oxygen species and ester groups in mechanisms of methane formation from pectin. Plant Cell Environ. 32, 1–9.
Milewska-Hendel, A., Sala, K., Gepfert, W., Kurczyńska, E., 2021. Gold nanoparticles-induced modifications in cell wall composition in *Barley* roots. Cells 10, 1965.
Milewska-Hendel, A., Witek, W., Rypień, A., Zubko, M., Baranski, R., Stróż, D., Kurczyńska, E.U., 2019. The development of a hairless phenotype in barley roots treated with gold nanoparticles is accompanied by changes in the symplasmic communication. Sci. Rep. 9.
Milewska-Hendel, A., Zubko, M., Karcz, J., Stróż, D., Kurczyńska, E., 2017. Fate of neutral-charged gold nanoparticles in the roots of the *Hordeum vulgare* L. cultivar Karat. Sci. Rep. 7.
Miralles, P., Church, T.L., Harris, A.T., 2012. Toxicity, uptake, and translocation of engineered nanomaterials in vascular plants. Environ. Sci. Technol. 46, 9224–9239.
Moghaddasi, S., Fotovat, A., Karimzadeh, F., Khazaei, H.R., Khorassani, R., Lakzian, A., 2017. Effects of coated and non-coated ZnO nano particles on cucumber seedlings grown in gel chamber. Arch. Agron. Soil Sci. 63, 1108–1120.
Molnár, Á., Rónavári, A., Bélteky, P., Szőllősi, R., Valyon, E., Oláh, D., Rázga, Z., Ördög, A., Kónya, Z., Kolbert, Z., 2020. ZnO nanoparticles induce cell wall remodeling and modify ROS/RNS signalling in roots of *Brassica* seedlings. Ecotoxicol. Environ. Saf. 206, 111158.
Mousavi Kouhi, S.M., Lahouti, M., Ganjeali, A., Entezari, M.H., 2014. Comparative phytotoxicity of ZnO nanoparticles, ZnO microparticles, and Zn^{2+} on rapeseed (*Brassica napus* L.): investigating a wide range of concentrations. Toxicol. Environ. Chem. 96, 861–868.
Naseer, S., Lee, Y., Lapierre, C., Franke, R., Nawrath, C., Geldner, N., 2012. Casparian strip diffusion barrier in *Arabidopsis* is made of a lignin polymer without suberin. Proc. Natl. Acad. Sci. USA 109, 10101–10106.
Nair, P.M.G., Chung, I.M., 2015. Study on the correlation between copper oxide nanoparticles induced growth suppression and enhanced lignification in Indian mustard (*Brassica juncea* L.). Ecotoxicol. Environ. Saf. 113, 302–313.
Nikonorova, N., Murphy, E., Fonseca De Lima, C.F., Zhu, S., van de Cotte, B., Vu, L.D., Balcerowicz, D., Li, L., Kong, X., De Rop, G., Beeckman, T., Friml, J., Vissenberg, K., Morris, P.C., Ding, Z., De Smet, I., 2021. The *Arabidopsis* root tip (phospho) proteomes at growth-promoting versus growth-repressing conditions reveal novel root growth regulators. Cells 10, 1665.
Park, Y.B., Cosgrove, D.J., 2012. Changes in cell wall biomechanical properties in the xyloglucan-deficientxxt1/xxt2 mutant of *Arabidopsis*. Plant Physiol. 158, 465–475.
Peng, C., Duan, D., Xu, C., Chen, Y., Sun, L., Zhang, H., Yuan, X., Zheng, L., Yang, Y., Yang, J., Zhen, X., Chen, Y., Shi, J., 2015. Translocation and biotransformation of CuO nanoparticles in rice (*Oryza sativa* L.) plants. Environ. Pollut. 197, 99–107.
Pfaffl, M.W., 2001. A new mathematical model for relative quantification in real-time RT-PCR. Nucleic Acids Res 29, e45.
Rossi, L., Zhang, W., Ma, X., 2017. Cerium oxide nanoparticles alter the salt stress tolerance of *Brassica napus* L. by modifying the formation of root apoplastic barriers. Environ. Pollut. 229, 132–138.
Schindler, T., Bergfeld, R., Schopfer, P., 1995. Arabinogalactan proteins in maize coleoptiles: developmental relationship to cell death during xylem differentiation but not to extension growth. Plant J. 7, 25–36.
Sénéchal, F., Wattier, C., Rustérucci, C., Pelloux, J., 2014. Homogalacturonan-modifying enzymes: structure, expression, and roles in plants. J. Exp. Bot. 65, 5125–5160.
Shi, J., Peng, C., Yang, Y., Yang, J., Zhang, H., Yuan, X., Chen, Y., Hu, T., 2014. Phytotoxicity and accumulation of copper oxide nanoparticles to the Cu-tolerant plant *Elsholtzia splendens*. Nanotoxicology 8, 179–188.
Sun, C., Lu, L., Liu, L., Liu, W., Yu, Y., Liu, X., Hu, Y., Jin, C., Lin, X., 2014. Nitrate reductase-mediated early nitric oxide burst alleviates oxidative damage induced by aluminum through enhancement of antioxidant defenses in roots of wheat (*Triticum aestivum*). New Phytol. 201, 1240–1250.
Van, A.R., Vanholme, R., Storme, V., Mortimer, J.C., Dupree, P., Boerjan, W., 2013. Lignin biosynthesis perturbations affect secondary cell wall composition and saccharification yield in *Arabidopsis thaliana*. Biotechnol. Biofuels 6, 46.
Van Sandt, V.S.T., Suslov, D., Verbelen, J., Vissenberg, K., 2007. Xyloglucan endotransglucosylase activity loosens a plant cell wall. Ann. Bot. 100, 1467–1473.
Verma, S.K., Das, A.K., Patel, M.K., Shah, A., Kumar, V., Gantait, S., 2018. Engineered nanomaterials for plant growth and development: a perspective analysis. Sci. Total Environ. 630, 1413–1435.
Verhertbruggen, Y., Marcus, S.E., Haeger, A., Ordaz-Ortiz, J.J., Knox, J.P., 2009. An extended set of monoclonal antibodies to pectic homogalacturonan. Carbohydr. Res. 344, 1858–1862.
Wang, W., Ren, Y., He, J., Zhang, L., Wang, X., Cui, Z., 2020. Impact of copper oxide nanoparticles on the germination, seedling growth, and physiological responses in *Brassica pekinensis* L. Environ. Sci. Pollut. R. 27, 31505–31515.
Wang, Z., Xie, X., Zhao, J., Liu, X., Feng, W., White, J.C., Xing, B., 2012. Xylem- and phloem-based transport of CuO nanoparticles in maize (*Zea mays* L.). Environ. Sci. Technol. 46, 4434–4441.
Wu, X., Song, H., Guan, C., Zhang, Z., 2020. Boron mitigates cadmium toxicity to rapeseed (*Brassica napus*) shoots by relieving oxidative stress and enhancing cadmium chelation onto cell walls. Environ. Pollut. 263, 114546.
Xiao, Y., Wu, X., Liu, D., Yao, J., Liang, G., Song, H., Ismail, A.M., Luo, J., Zhang, Z., 2020. Cell wall polysaccharide-mediated cadmium tolerance between two *Arabidopsis thaliana* ecotypes. Front. Plant Sci. 11.
Xiao, Z., Yue, L., Wang, C., Chen, F., Ding, Y., Liu, Y., Cao, X., Chen, Z., Rasmann, S., Wang, Z., 2021. Downregulation of the photosynthetic machinery and carbon storage signaling pathways mediate La_2O_3 nanoparticle toxicity on radish taproot formation. J. Hazard. Mater. 411, 124971.
Xie, Q., Essemine, J., Pang, X., Chen, H., Cai, W., 2020. Exogenous application of abscisic acid to shoots promotes primary root cell division and elongation. Plant Sci. 292, 110385.
Xiong, T., Dumat, C., Dappe, V., Vezin, H., Schreck, E., Shahid, M., Pierart, A., Sobanska, S., 2017. Copper oxide nanoparticle foliar uptake, phytotoxicity, and consequences for sustainable urban agriculture. Environ. Sci. Technol. 51, 5242–5251.
Yang, J.L., Zhu, X.F., Peng, Y.X., Zheng, C., Li, G.X., Liu, Y., Shi, Y.Z., Zheng, S.J., 2011. Cell wall hemicellulose contributes significantly to aluminum adsorption and root growth in *Arabidopsis*. Plant Physiol. 155, 1885–1892.
Yuan, J., He, A., Huang, S., Hua, J., Sheng, G.D., 2016. Internalization and phytotoxic effects of cuo nanoparticles in *Arabidopsis thaliana* as revealed by fatty acid profiles. Environ. Sci. Technol. 50, 10437–10447.
Yue, L., Chen, F., Yu, K., Xiao, Z., Yu, X., Wang, Z., Xing, B., 2019. Early development of apoplastic barriers and molecular mechanisms in juvenile maize roots in response to La_2O_3 nanoparticles. Sci. Total Environ. 653, 675–683.
Zhang, J., Zhang, L., Wei, Y., Ma, J., Shuang, S., Cai, Z., Dong, C., 2014. A selectively fluorescein-based colorimetric probe for detecting copper (II) ion. Spectrochim. Acta Part A Mol. Biomol. Spectrosc. 122, 731–736.
Zhu, X.F., Shi, Y.Z., Lei, G.J., Fry, S.C., Zhang, B.C., Zhou, Y.H., Braam, J., Jiang, T., Xu, X.Y., Mao, C.Z., Pan, Y.J., Yang, J.L., Wu, P., Zheng, S.J., 2012. *XTH31*, encoding an in vitro XEH/XET-active enzyme, regulates aluminum sensitivity by modulating in vivo XET action, cell wall xyloglucan content, and aluminum binding capacity in *Arabidopsis*. Plant Cell 24, 4731–4747.
Zhu, X.F., Wan, J.X., Sun, Y., Shi, Y.Z., Braam, J., Li, G.X., Zheng, S.J., 2014. Xyloglucan endotransglucosylase-hydrolase17 interacts with xyloglucan endotransglucosylase-hydrolase31 to confer xyloglucan endotransglucosylase action and affect aluminum sensitivity in *Arabidopsis*. Plant Physiol. 165, 1566–1574.